Research Article | Vol. 8, No. 9 | 1 Sep 2017 | BIOMEDICAL OPTICS EXPRESS 4152
Biomedical Optics EXPRESS

Retinal imaging in human autopsy eyes using a custom optical coherence tomography periscope

RYAN P. MCNABB,[1,*] JAMES TIAN,[1] SINA FARSIU,[1,2] JOSEPH A. IZATT,[1,2] ELEONORA M. LAD,[1] AND ANTHONY N. KUO[1,2]

[1]*Department of Ophthalmology, Duke University Medical Center, 2351 Erwin Rd, Durham, NC 27705, USA*
[2]*Department of Biomedical Engineering, Duke University, 101 Science Drive, Durham, NC 27708, USA*
[*]*ryan.mcnabb@dm.duke.edu*

Abstract: Age-related macular degeneration (AMD) is a major cause of vision loss in the elderly. To better study the pathobiology of AMD, postmortem eyes offer an excellent opportunity to correlate optical coherence tomography (OCT) imaging characteristics with histopathology. However, postmortem eyes from autopsy present challenges to standard OCT imaging including opaque anterior segment structures and standard of care autopsy processing resulting in oblique views to the macula. To overcome these challenges, we report a custom periscope attached by a standard mount to an OCT sample arm and demonstrate high quality macular OCT acquisitions in autopsy-processed eyes.

OCIS codes: (170.4500) Optical coherence tomography; (170.0110) Imaging systems; (170.4470) Ophthalmology.

References and links

1. D. B. Rein, J. S. Wittenborn, X. Zhang, A. A. Honeycutt, S. B. Lesesne, and J. Saaddine; Vision Health Cost-Effectiveness Study Group, "Forecasting age-related macular degeneration through the year 2050: The potential impact of new treatments," Arch. Ophthalmol. **127**(4), 533–540 (2009).
2. P. P. Srinivasan, L. A. Kim, P. S. Mettu, S. W. Cousins, G. M. Comer, J. A. Izatt, and S. Farsiu, "Fully automated detection of diabetic macular edema and dry age-related macular degeneration from optical coherence tomography images," Biomed. Opt. Express **5**(10), 3568–3577 (2014).
3. S. Farsiu, S. J. Chiu, R. V. O'Connell, F. A. Folgar, E. Yuan, J. A. Izatt, and C. A. Toth, "Quantitative Classification of Eyes with and without Intermediate Age-related Macular Degeneration Using Optical Coherence Tomography," Ophthalmology **121**(1), 162–172 (2014).
4. "Age-Related Macular Degeneration, Preferred Practice Patern," (American Academy of Ophthalmology, 2015).
5. C. A. Curcio, J. D. Messinger, K. R. Sloan, A. Mitra, G. McGwin, and R. F. Spaide, "Human Chorioretinal Layer Thicknesses Measured in Macula-wide, High-Resolution Histologic Sections," Invest. Ophthalmol. Vis. Sci. **52**(7), 3943–3954 (2011).
6. N. H. Brown, A. F. Koreishi, M. McCall, J. A. Izatt, C. B. Rickman, and C. A. Toth, "Developing SDOCT to assess donor human eyes prior to tissue sectioning for research," Graefes Arch. Clin. Exp. Ophthalmol. **247**(8), 1069–1080 (2009).
7. N. Bagheri, B. A. Bell, V. L. Bonilha, and J. G. Hollyfield, "Imaging Human Postmortem Eyes with SLO and OCT," in *Retinal Degenerative Diseases*, M. M. LaVail, J. D. Ash, R. E. Anderson, J. G. Hollyfield, and C. Grimm, eds. (Springer US, Boston, MA, 2012), pp. 479–488.
8. J. A. Izatt and M. A. Choma, "Theory of Optical Coherence Tomography," in *Optical Coherence Tomography*, W. Drexler and J. Fujimoto, eds. (Springer Berlin Heidelberg, 2008), pp. 47–72.
9. R. P. McNabb, "DMLS_Periscope.STL" (2017), retrieved https://doi.org/10.6084/m9.figshare.4826737.
10. R. P. McNabb, F. Larocca, S. Farsiu, A. N. Kuo, and J. A. Izatt, "Distributed scanning volumetric SDOCT for motion corrected corneal biometry," Biomed. Opt. Express **3**(9), 2050–2065 (2012).
11. J. A. Izatt, M. R. Hee, G. M. Owen, E. A. Swanson, and J. G. Fujimoto, "Optical coherence microscopy in scattering media," Opt. Lett. **19**(8), 590–592 (1994).
12. W. Drexler, U. Morgner, R. K. Ghanta, F. X. Kärtner, J. S. Schuman, and J. G. Fujimoto, "Ultrahigh-resolution ophthalmic optical coherence tomography," Nat. Med. **7**(4), 502–507 (2001).
13. W. Drexler, H. Sattmann, B. Hermann, T. H. Ko, M. Stur, A. Unterhuber, C. Scholda, O. Findl, M. Wirtitsch, J. G. Fujimoto, and A. F. Fercher, "Enhanced visualization of macular pathology with the use of ultrahigh-resolution optical coherence tomography," Arch. Ophthalmol. **121**(5), 695–706 (2003).

#297254 https://doi.org/10.1364/BOE.8.004152
Journal © 2017 Received 1 Jun 2017; revised 9 Aug 2017; accepted 9 Aug 2017; published 21 Aug 2017

Biomedical Optics EXPRESS

14. S. J. Chiu, X. T. Li, P. Nicholas, C. A. Toth, J. A. Izatt, and S. Farsiu, "Automatic segmentation of seven retinal layers in SDOCT images congruent with expert manual segmentation," Opt. Express **18**(18), 19413–19428 (2010).
15. A. Unterhuber, B. Považay, B. Hermann, H. Sattmann, A. Chavez-Pirson, and W. Drexler, "In vivo retinal optical coherence tomography at 1040 nm - enhanced penetration into the choroid," Opt. Express **13**(9), 3252–3258 (2005).
16. O. O. Ahsen, Y. K. Tao, B. M. Potsaid, Y. Sheikine, J. Jiang, I. Grulkowski, T.-H. Tsai, V. Jayaraman, M. F. Kraus, J. L. Connolly, J. Hornegger, A. Cable, and J. G. Fujimoto, "Swept source optical coherence microscopy using a 1310 nm VCSEL light source," Opt. Express **21**(15), 18021–18033 (2013).
17. R. P. McNabb, D. S. Grewal, R. Mehta, S. G. Schuman, J. A. Izatt, T. H. Mahmoud, G. J. Jaffe, P. Mruthyunjaya, and A. N. Kuo, "Wide field of view swept-source optical coherence tomography for peripheral retinal disease," Br. J. Ophthalmol. **100**(10), 1377–1382 (2016).

1. Introduction

Age-related macular degeneration (AMD) is the leading cause of irreversible vision loss in Americans over 60 years of age and will become increasingly common in the aging world population [1]. Its late stage is classified as either atrophic (dry) AMD with geographic atrophy or exudative (wet) AMD with choroidal neovascularization. To help diagnose and longitudinally follow AMD clinically, optical coherence tomography (OCT) is widely used in eye care for the detailed cross-sectional retinal morphology that it provides [2]. OCT-derived retinal thickness and retinal pigment epithelium drusen complex (RPEDC) maps are clinically used for determining disease stage, atrophy and exudation, and the information from the RPEDC map has been correlated with risk of clinical progression [3].

However, significant gaps still exist in our understanding of the pathobiology of AMD as is evident by a current lack of treatment for the great majority of patients affected with the atrophic (dry) form of the disease [4]. Further, the current *en face* photography classification system does not account for the recent technological advances in retinal imaging and histopathology. Hence, there is a need to robustly characterize the changes seen in high-resolution retinal imaging of AMD with the underlying biological changes seen in histopathology. Postmortem donor eyes offer an opportunity to perform both histopathology and OCT imaging and thus correlate the two modalities [5]. Limited earlier work has demonstrated the benefits of OCT imaging in a small number of donor eyes. OCT can produce *en face* retinal images comparable to corresponding postmortem photographs of the retina taken with a dissection microscope [6]. In addition, OCT may be valuable as a screening tool for staging retinal disease for postmortem research studies, for circumscribing the area for tissue sectioning, and correcting erroneous or missing clinical records [6, 7].

While this limited body of work in postmortem donor eyes is promising, larger studies are needed to correlate specific disease biology and features seen in AMD histopathology with their appearance on OCT imaging. A more extensive source of postmortem eyes is from autopsy cases. Access to this larger source increases the opportunity of identifying eyes afflicted with various stages of AMD and matched controls to properly perform large imaging and histopathologic correlation studies. The challenge of autopsy eyes is that they are prepared using a standardized, mandatory standard of care process that is not conducive to standard OCT imaging. Unlike donor eyes where the clouded cornea and lens can be removed postmortem, to provide direct optical access to the posterior segment, autopsy eyes are required to be prepared by sectioning the superior and inferior calottes (the superior and inferior third of the eye are sectioned along the horizontal or axial plane; see Fig. 1(A) for a diagram of a superior calotte). This process leaves the visual axis intact for pathology examination, but this does not provide optical access to the macula given postmortem clouding of the cornea and lens. This is in contrast to the *in vivo* clear cornea and lens. Further, the diameter of the superior and inferior openings from the calotte are too small to allow introduction of a regular OCT sample arm probe; if the sample arm probe is external, only oblique imaging through the calotte opening onto the macula is possible.

Biomedical Optics EXPRESS

To address these challenges, we describe in this work a custom periscope which can be attached by a standard mount to an OCT sample arm. This custom periscope is small enough to be introduced through the calotte openings of an autopsy prepared eye and allows the OCT system to telecentrically image the postmortem macula with high resolution, while an aiming laser beam allows precise external visualization and localization of the OCT beam on the retina.

2. Methods

2.1 Optical system

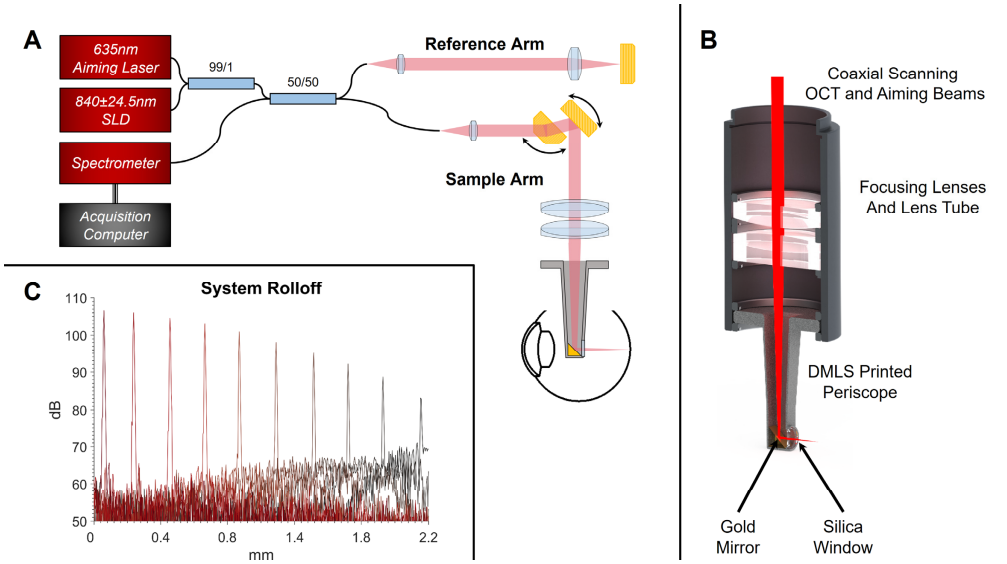

Fig. 1. *A)* Spectral domain OCT system schematic with custom periscope bore *B)* Cut away view of Solidworks rendering of custom periscope bore *C)* System rolloff performance.

We developed our imaging system (Fig. 1(A)) utilizing a commercial SDOCT system (Bioptigen, Inc., Durham, NC) centered at $\lambda = 840$ nm, $\Delta\lambda = 49$ nm and modified to include a coaxial visible aiming laser (S1FC635; Thorlabs, Inc.). This gives a theoretical axial resolution of the system of 6.4 µm in air and 4.8 µm in tissue ($n = 1.337$) [8]. This system utilizes a handheld, portable probe that contains fiber connection, collimation optics, and offset orthogonal scanning galvanometers. The final imaging optics are contained in interchangeable bores for different imaging environments. The optics for our custom postmortem eye imaging bore consists of two achromatic lenses (AC254-100-B, AC254-150-B; Thorlabs, Inc.), a gold turn mirror (MRA05-M01; Thorlabs, Inc.) and an uncoated fused silica window (#47-833; Edmund Optics, Inc.). The opto-mechanics consist of a stock lens tube (SM1L20; Thorlabs, Inc.), retaining rings (SM1RR; Thorlabs, Inc.), a thread adapting ring between the lens tube and handheld probe, and a custom cobalt chrome direct metal laser sintered (DMLS) periscope bore for which we provide the .STL file (Ref [9].). A Solidworks rendering of the custom bore can be seen in Fig. 1(B).

Following printing of the periscope mechanic, the gold turn mirror was placed within the periscope and epoxied at the bottom with the hypotenuse facing the window opening. Once the mirror was in place, we tested the imaging system for correct alignment. Following testing, we epoxied the uncoated fused silica window into its correct location taking care to ensure that we formed a complete seal around the window to prevent leakage into the bore. After the epoxy cured, we placed the tip of the periscope into water such that the window was completely submerged. Upon removal, we inspected for any leakage.

Biomedical Optics EXPRESS

The imaging depth of the complete system was 2.2mm in air (Fig. 1(C)) with a peak sensitivity of 106.3 dB at an A-scan repetition rate of 20 kHz and 640 µW of optical power incident at the sample. We placed a mirror (in air) at the imaging plane of the bore and moved the reference arm to measure rolloff. We placed a neutral density filter between the mirror and the bore to attenuate the signal below camera saturation. This performance is similar to the previously reported values of this same SDOCT engine when utilizing a telecentric imaging bore [10].

2.2 Imaging protocol

All eyes were obtained from the Duke University Hospital Department of Pathology, and all eyes were fixed in 3.7% neutral-buffered paraformaldehyde prior to handling. A larger time-to-fixation interval in postmortem eyes results in autolysis, tissue destruction, and increased processing and imaging artifacts, making visualization of specific pathologies more difficult. To limit these issues, all eyes in this study were fixed within 36 hours postmortem. The use of autopsy eyes for research was approved by the Institutional Review Board of Duke University, and followed the tenets of the Declaration of Helsinki. We imaged 36 eyes from 22 subjects. Prior to imaging, we performed a partial vitrectomy on the postmortem eyes to remove vitreous that may interfere with placement of the periscope within the eye. We then placed the postmortem eyes in a buffered saline solution (BSS) bath within a shallow plastic container such that the calotte opening faced the top of the bath. The BSS bath provided a homogenous medium for imaging in order to avoid the presence of separate zones of air and residual fluid. We placed the BSS bath on a mounted 5-axis stage (562 Series; Newport, Inc.) to provide fine sample placement and we mounted the handheld probe on a fixed, coarse axial stage that allowed lowering of the periscope through the calotte of the postmortem eye. We then visually aligned the eye such that the aiming laser intersected the region of interest within the eye.

We utilized two scan protocols for imaging postmortem eyes: volumes and repeated B-scans. For both scan protocols, A-scans were 512 pixels in length. Volumes consisted of 500 A-scans per B-scan and 500 B-scans per volume over a rectangular scan area of 4mm x 4mm and limited by the 4mm diameter aperture of the window opening of the periscope. Repeated B-scans consisted of 1000 A-scans per B-scan and 100 repeated B-scans over a 4mm length. Depending on the specimen, we utilized both sides of DC placing the structure of interest in the region with the highest sensitivity and correcting for dispersion differences in software. Following imaging with OCT, the eyes were embedded in paraffin and sectioned at 5 µm. Hematoxylin and eosin (H&E) stains were performed on pupil-optic nerve sections of the globes, and slides evaluated for presence of AMD and other ocular conditions.

Matching histological slides to OCT slices was an iterative process that began during OCT volumetric imaging of the postmortem eye. Due to the small size of the periscope relative to the opening provided by the calotte, ocular structures such as the foveal region, optic nerve head or any other regions of interest could be seen around the periscope. By utilizing the visible aiming laser, OCT image acquisition could be further and more precisely guided to structures of interest. Following paraffin embedding and sectioning of the postmortem eyes, histopathology analysis and imaging of the individual slides from the region of interest were performed. Because OCT volumes collect data over a known area, the clinical pathologist paired these histological images with correlated OCT slices from the previously acquired volume.

For comparison of the above engine and scan protocols with normal *in vivo* retinal imaging, we swapped the custom periscope bore for the commercial retinal imaging bore (Bioptigen, Inc., Durham, NC) provided with the system that additionally provides the ability to correct for the Diopter defocus of a subject. With this setup, we imaged a single, normal subject (27 years old) who was consented under a Duke University IRB approved protocol.

Biomedical Optics EXPRESS

3. Results

3.1 Differences in OCT imaging of retina in autopsy eyes

One advantage of OCT over confocal microscopy is that system axial resolution is not typically limited by the confocal gate of the imaging system but is instead a function of the detected bandwidth of the imaging spectrum [11]. Because of this principle, OCT has become a standard ophthalmic imaging technique due to its ability to detect retinal layers *in vivo*. In Fig. 2 we show OCT images from an *in vivo* retina centered at the fovea (Fig. 2(A); layer terminology adapted from [12–14]) and a separate (not same individual) retina centered at the fovea from an autopsy eye. We imaged the autopsy eye with the same engine as the *in vivo* eye, only with the described periscope sample arm attachment. The axial resolution of the two systems is the same; however, there is a noticeable loss of the typical inner retinal layers in the autopsy eye due to inner retinal opacification as a postmortem artifact (Fig. 2(B)). In addition, the fovea of postmortem eyes is often characterized by a typical folding of the retina (Fig. 2(B)).

The loss of retinal layers and other structural artifacts were common throughout the autopsy-prepared eyes imaged. In Fig. 2(B), the boundaries between the remaining vitreous and retina (upper right), the boundary between the outer plexiform and outer nuclear layers (intra-retinal transition from bright to dark), and the boundary between the outer retina and the retinal pigment epithelium (RPE) are all visible. Other intra-retinal layers were more variably defined in these postmortem images (compare Fig. 2(B) to Fig. 3(A)). The RPE typically presents as highly scattering layers in the living eye (Fig. 2(A)) but following fixation there was a degradation of this and other layered structures across the autopsy eyes imaged.

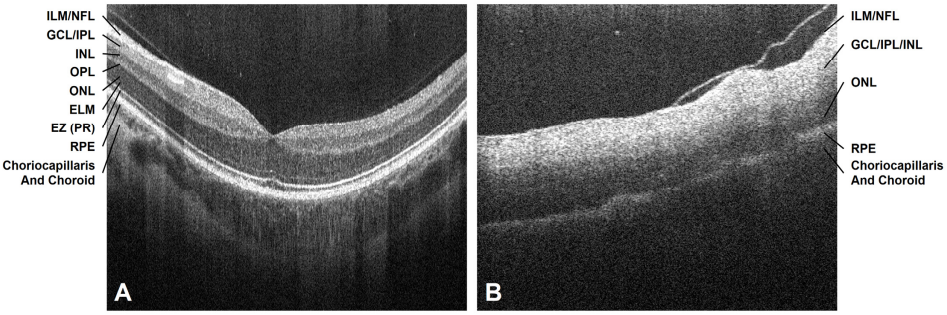

Fig. 2. *A) In vivo* retinal image with above described OCT engine and retinal imaging bore; ILM/NFL – Inner limiting membrane and nerve fiber layer; GCL/IPL – Ganglion cell layer and inner plexiform layer; INL – Inner nuclear layer; OPL – Outer plexiform layer; ONL – Outer nuclear layer; ELM – External limiting membrane; EZ (PR) – Ellipsoidal Zone (Photoreceptor layer) *B)* Separate autopsy prepared eye imaged with periscope bore and same engine as *A*. Following fixation of the postmortem eye, there was a degradation of retinal layer differentiation. Both *A* and *B* exhibit local detachment of the vitreous from the retina.

Biomedical Optics EXPRESS

3.2 OCT and histology

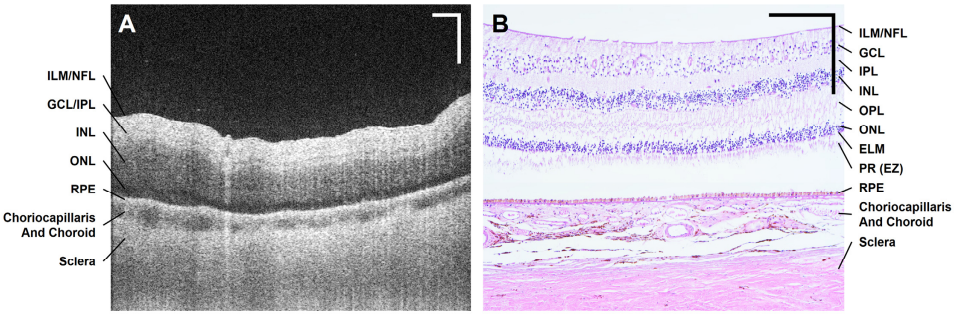

Fig. 3. *A)* OCT image utilizing custom periscope on normal autopsy retina *B)* Montage of corresponding histology images where retina had artifactually detached from the RPE during sectioning. Scale bars are 250μm for all images.

Figure 3 shows a normal, autopsy retina as imaged with the periscope OCT (Fig. 3(A)) and its corresponding histopathology (Fig. 3(B)). The various retinal layers are visible in the OCT image, and a distinct boundary between the retina and the intact choroid is seen. Figure 3(B) is a montage of two images, one of the retina and the second of the RPE and choroid, of the same sample. During processing, the retina commonly detaches from the RPE as well as the underlying choroid and sclera, as in this case. While the images were montaged together to create Fig. 3(B) for illustrative purposes, this highlights the structural artifacts that are common with histopathology that are not present in OCT.

Figure 4 shows three separate eyes, each with their own paired OCT and histopathology. In all histopathology images, the retina has detached from the RPE but could be photographed in the same image. Figures 4(A) and 4(B) shows an eye with peripheral cystoid degeneration and its characteristic paving stone morphology. We took this OCT volume slice (and corresponding histopathology) from a section of the peripheral retina that was close to the ora serrate. The ability to image the extreme retinal periphery is an advantage of utilizing a periscope over a more conventional method of imaging with the native ocular optics and corresponding visual axis. For this set of images, the tissue placement on the histological slide was rotated relative to the periscope imaging plane. Both Figs. 4(C) and 4(D) and 4(E) and 4(F) are from a more conventional region of interest near the macula. Figures 4(C) and 4(D) are from a subject that had AMD with associated calcified drusen (arrows), while Figs. 4(E) and 4(F) are from an eye with subretinal fluid associated with exudative AMD. Both OCT and histopathology show fixation artifacts. The OCT image shows postmortem folding of the retina. In the histopathology image, the sample is stained and mounted and as a result, the retina is no longer attached to the RPE but the folding appears to have been smoothed.

Biomedical Optics EXPRESS

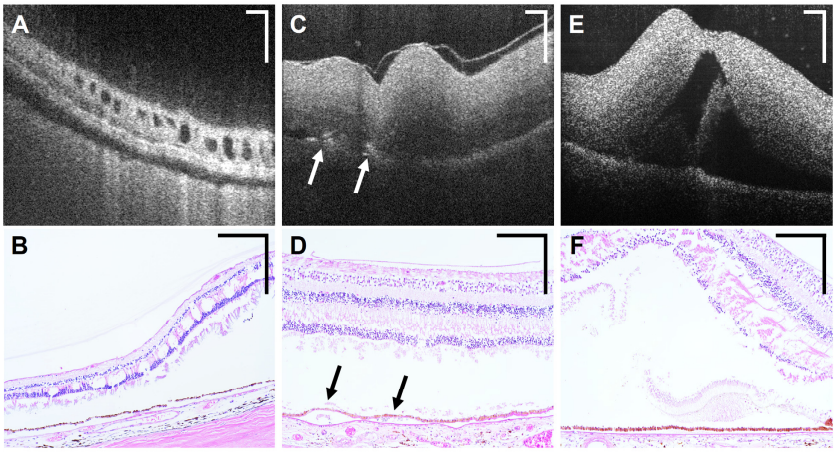

Fig. 4. *A&B)* Correlated OCT and histology images from eye with peripheral cystoid degeneration *C&D)* Correlated images from eye with age-related macular degeneration and calcified drusen (arrows) *E&F)* Correlated images from eye with sub-retinal fluid. See Visualization 1 for OCT volume. Scale bars are 250µm for all images.

4. Discussion and conclusion

Imaging of postmortem eyes is critically important for studying macular degeneration and other retinal conditions as it allows a direct correlation between imaging characteristics and histopathology in the same eye. However, postmortem eyes present unique challenges to standard OCT imaging. Specifically, postmortem eyes processed using standard autopsy protocols remove the superior and inferior poles of the eye along the axial plane (calottes). This protocol results in an anterior-optic nerve slice through the entire eye. The tissue slice is then paraffin embedded and sectioned at 5µm allowing for sections through the entire globe such that these sections include the cornea, iris, lens, macula and optic nerve all together. Following staining, these sections are examined by a clinical ophthalmic pathologist, who is then able to render all ophthalmic clinical diagnoses present in the autopsy eye. Relevant OCT imaging should be performed following the formation of the calottes but prior to the embedding and sectioning. This autopsy preparation protocol requires that the visual axis remain intact, and the postmortem cornea and lens typically are not transmissive enough to allow OCT imaging through the intact but clouded visual axis. Alternatively, imaging through the open calottes forces undesirably oblique imaging of the macula given the position of the calottes superior and inferior to the macula. In this work, we have described and demonstrated a periscopic OCT sample arm attachment that addresses these challenges to produce high quality OCT macular images of postmortem eyes processed using standard autopsy protocols. The periscopic OCT attachment fits easily through the calottes and redirects the OCT scan to allow telecentric imaging on the macula despite the superior (or inferior) approach through the calottes. Given the flexibility of the periscope within the eye, more peripheral regions were also easily accessed (Fig. 4(A)). Compared to histopathologic images of the same eyes, the images from the periscopic OCT attachment correspond well with the underlying anatomy from histopathology.

The STP file to reproduce the periscopic OCT attachment are provided in Ref [9]. The periscopic OCT attachment should be placed subsequent to the scanning mirrors in collimated space. Though high quality images have been obtained with this attachment as is, minor modifications could be made to further improve image quality. For example, the uncoated fused silica window serves as a separating interface between the BSS and the air within the bore. An obvious solution to improve performance might be to utilize a window with an anti-reflective (AR) coating to reduce the reflections from the air-silica interface. However, we did

Biomedical Optics EXPRESS

attempt this in a previous iteration of the periscope and the reflections caused by the interface between the stock AR coating and the BSS dominated such that imaging was untenable with that bore. By moving to a custom window we could obtain a custom shape and material, select an appropriate anti-reflection coating for the air side of the window and either leave the imaging side of the window uncoated or provide an anti-reflection coating that worked with BSS. For cleaning purposes, there is value in leaving the BSS-window interface uncoated. To improve imaging depth into subretinal structures, using a current generation swept-source OCT engine in the 1050nm or 1310nm regimes would allow for greater penetration into the tissue by virtue of the longer source wavelengths [15, 16]. Additionally, the improved falloff and imaging depth, coupled with an optical design with a larger field-of-view, could also allow for imaging of larger retinal pathologies [17]. Despite this, we have demonstrated that high quality images can be acquired using this attachment on an available spectral domain OCT engine.

With this periscopic OCT attachment, postmortem eyes that have been prepared according to standard of care autopsy protocols can be readily used for OCT imaging – histopathologic correlation studies. The provided CAD drawing should allow reproduction and modification of the attachment for others to use and advance studies to relate imaging biomarkers with their anatomic correlates in important retinal diseases such as macular degeneration.

Funding

We acknowledge support from the National Institutes of Health (R01-EY024312, R21-EY025427, R01-EY023039, 5K12-EY016333-08) and Research to Prevent Blindness Ernest & Elizabeth Althouse Special Scholar Award.

Acknowledgments

The authors thank Alan D. Proia, MD, PhD (Dept of Pathology, Duke University) for his assistance in accessing the autopsy eyes and for histopathology guidance.

Conflicts of Interest

RPM: Leica Microsystems, Inc. (P), JT: None, SF: None, JAI: Leica Microsystems, Inc. (P, R), EML: None, ANK: Leica Microsystems, Inc. (P)